Indian Journal of Pure & Applied Physics
Vol. 56, February 2018, pp. 149-157

A polarization insensitive ultrathin compact triple band metamaterial absorber

D Sood* & C C Tripathi
University Institute of Engineering & Technology, Kurukshetra University, Kurukshetra 136 119, India

Received 14 September 2016; accepted 31 October 2017

In this paper, design, characterization and measurements of an ultrathin compact polarization insensitive triple band metamaterial absorber for wide incident angle have been presented. The unit cell design consists of a Jerusalem cross shaped resonator inside a square loop resonator. The proposed absorber exhibits triple band absorption at 4.4, 6.48 and 15.44 GHz with 96.6% and 97.64% and 85.81% absorptivity, respectively, for wide incident angles of electromagnetic wave. The absorption frequencies can be effectively adjusted for C, X and Ku frequency bands by optimizing the dimensions of the absorber design. The proposed absorber is ultrathin (0.014 λ_0) in thickness and compact (0.12 λ_0) in size at the lowest frequency of absorption. The proposed absorber exhibits TE and TM polarization stability and provides high absorption up to the incident angle of 60°. A prototype of the proposed absorber structure has been fabricated and experimentally tested for normal and oblique incidences for TE and TM polarization. The measured responses have been observed in agreement with the simulated ones.

Keywords: Metamaterial absorber, Triple band, Compact, Ultra-thin, Polarization insensitive, Microwave absorber.

1 Introduction

Metamaterials are periodic composite structures with unusual, attractive properties[1], i.e., negative effective permittivity and permeability, which make them a potential candidate to serve various useful applications such as cloaking[2], perfect lens[3], antennas[4], imaging[5] and absorber[6]. In recent years, metamaterial based absorbers have drawn considerable attention of researchers due to their almost perfect absorption, ultrathin thickness, ease of fabrication and flexibility to control absorption frequencies.

Metamaterial based absorbers consist of periodic arrays of frequency selective metallic patterns printed on the top of a metal grounded dielectric substrate. The top, metallic pattern is excited by the incident electric field and the dielectric substrate is excited by the incident magnetic field[6]. This interaction of electromagnetic field tunes the effective permittivity and permeability of the structure in such a way that the input impedance of the structure becomes equal to the free space impedance which minimizes the reflection from the absorber.

In spite of these effective and useful properties, the metamaterial absorbers suffer from certain deficiencies such as narrow absorption bandwidth, polarization sensitivity, large unit cell size, etc. After the development of the first metamaterial based absorber[6] different approaches have been adopted to improve the performance of the metamaterial based absorbers in terms of multiband operation, ultrathin thickness, compact size, bandwidth enhancement and polarization insensitivity, etc. Initial techniques to design polarization and incident angle insensitive absorber have been reported in literature[7,8]. Performance advancement through the design of dual band[9] and multiband absorber[10] has been suggested. Various approaches to design triple band metamaterial absorber have also been reported[11-18]. A triple band absorber design is presented by Xu *et al.*[12] but it does not provide the flexibility to control the individual absorption frequencies. The use of multiple copies of the same resonator in a single unit cell is another technique to achieve multiband absorption, but the large unit cell size is its major limitation[10,11]. Triple band absorbers reported in literature[12-16] have larger unit cell size and do not provide separate control of absorption frequencies. Closed ring resonator (CRR) based metamaterial absorbers have been attracted much attention due their symmetric design configuration[16]. A multilayer absorber structure has also been reported[18] to achieve multiband absorption, but the fabrication overhead and alignment of multiple layers limits its practical use. Therefore, easier techniques to design an ultrathin, compact, polarization insensitive multiband absorber with the flexibility to control individual absorption frequencies are required.

*Correponding author (E-mail: deepaksood.uiet@gmail.com)

In this paper, an ultrathin compact polarization insensitive triple band metamaterial absorber with flexibility to separately adjust the absorption frequencies has been presented. The proposed absorber exhibits three absorption peaks. It is polarization insensitive and exhibits a high absorption for wide incident angle up to 60° for oblique incidence of electromagnetic wave. Surface current and field distributions have been studied in order to understand the mechanism of absorption in the proposed absorber. The contribution of dimensional parameters of the individual resonators has been analysed to understand the origin of absorption peaks. Further, the control of absorption frequencies through optimization of the overall dimensions of the inner JCS resonator has been demonstrated. A prototype of the proposed absorber has been fabricated on a 1 mm thick FR–4 substrate. The fabricated structure has been experimentally tested for normal and oblique incidence angles for both TE and TM polarization. From the results it is observed that the proposed absorber is polarization insensitive and provides triple band absorption for wide incident angles. These features make it useful for different RF applications such as RCS reduction, electromagnetic interference shielding and in bolometer, etc.

2 Unit Cell Design

The top view of the proposed absorber design along with the directions of electric vector, magnetic vector and direction of propagation is shown in Fig. 1. The optimized dimensions are P = 8.2 mm, L = 7.8 mm, L_1 = 5.0 mm, L_2 = 2.55 mm, W = 0.3 mm. The unit cell consists of a Jerusalem cross resonator within a concentric square loop resonator as the top metal layer on a 1 mm thick FR-4 dielectric substrate permittivity ε_r = 4.4 and tanδ = 0.02. The bottom layer is completely metal laminated. The top and bottom layers are made up of copper ($\sigma = 5.2 \times 10^7$ S/m) of thickness 0.03 mm.

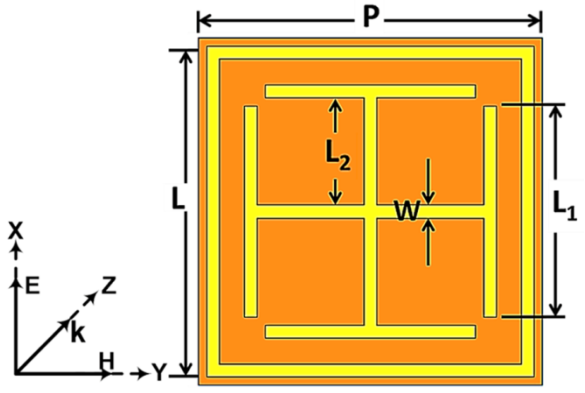

Fig. 1 — Unit cell design of the proposed absorber (P = 8.2 mm, L = 7.8 mm, L_1 = 5.0 mm, L_2 = 2.55 mm, W = 0.3 mm).

3 Simulation

In order to simulate an infinite array of the proposed absorber Floquet periodic boundary conditions in 'X' and 'Y' directions are applied using ANSYS's HFSS software tool. The absorptivity (A) is determined as per Eq. (1):

$$A = 1 - |S_{11}|^2 - |S_{21}|^2 \quad \ldots (1)$$

Here, $|S_{11}|^2$ and $|S_{21}|^2$ represents reflected and transmitted power, respectively. As the bottom surface is completely copper laminated so there is no transmission power, i.e., $|S_{21}|^2 = 0$. Therefore, the absorptivity is calculated from the reflected power only. The simulation response under normal incidence of the incoming wave is shown in Fig. 2. It is observed that the proposed absorber exhibits three distinct absorption peaks (f_1, f_2 and f_3) at 4.4, 6.48 and 15.44 GHz with 96.6% and 97.64% and 87.44% absorptivity, respectively.

3.1 Simulated response under different polarization angles

The performance of the absorber structure has been studied at different polarization angles (ϕ) from 0° to 90°. When the electric field (E) and magnetic field (H) are at some angle ϕ with respect to X-axis and Y-axis, respectively, keeping the direction of propagation fixed along Z-axis then the polarization of incoming wave changes. The top layer of the absorber structure has been designed with fourfold symmetric configuration so that it provides polarization insensitivity. The simulation response under normal incidence for different angles of polarization is shown in Fig. 3.

3.2 Simulated response under different oblique incidence angles

The absorber has also been studied for different oblique incidence angles for both TE and TM polarization. In TE polarization the electric field is

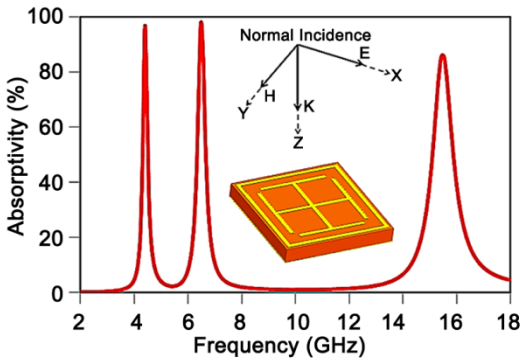

Fig. 2 — Simulated absorptivity response under normal incidence.

along *X*-axis and the magnetic field is at some angle with respect to *Y*-axis such that the direction of the incident wave is inclined by an angle θ with *Z*-axis. The simulated absorptivity response of the proposed triple band absorber for different oblique incidence angles under TE polarization is shown in Fig. 4. It is observed that the absorptivity of more than 80% has been achieved with wide incident angle stability up to the incident angle (θ) of 60°. The proposed design is geometrically symmetric and compact in size, therefore the similar performance of the proposed absorber has been noticed for TM polarization for different oblique incidence angles as shown in Fig. 5. In TM polarization, the magnetic field is along the *Y*-axis and the electric field is at some angle with respect to *X*-axis such that the direction of the incident wave is inclined by an angle θ with Z-axis.

4 Absorption Mechanism

In order to understand the physical mechanism of absorption, the field and surface current distributions have been studied for the three absorption peaks. From the field distribution as illustrated in Fig. 6(a), it is observed that the outer square loop resonator is the primary contributor for the first absorption frequency (f_1) of 4.4 GHz, as high electric and magnetic fields are distributed around it. However, the other two absorption frequencies are mainly contributed by the inner JCS resonator. At the second absorption peak (f_2) of 6.48 GHz, the electric and magnetic fields are mainly distributed across the vertical and horizontal arms of the portion I of the JCS resonator, respectively, as shown in Fig. 6(b). At the third absorption frequency (f_3) of 15.44 GHz the horizontal arms of the portion II of the inner JCS resonator contributes highly as shown in Fig. 6(c).

The surface current distributions for the three absorption frequencies have also been shown in Fig. 7. Similar to the observations of field distributions, it is noticed that f_1 is primarily contributed by the outer square loop as the surface current is mainly distributed over the outer square loop at this frequency as shown in Fig. 7(a). Further, f_2 is contributed by the portion I of the inner JCS resonator as the surface current is mainly distributed across it as shown in Fig. 7(b) while at f_3 the surface current is mainly distributed at the portion II of the inner resonator as shown in Fig. 7(c). For all the three absorption frequencies the surface currents are antiparallel at the top and bottom surface. The antiparallel currents form the circulating loops around the incident magnetic field. This strong coupling of electric and magnetic field with the top, metallic pattern and dielectric substrate respectively realizes the high absorption.

To observe the contribution of inner and outer resonators in absorption, the variation of their essential dimensional parameters has been studied.

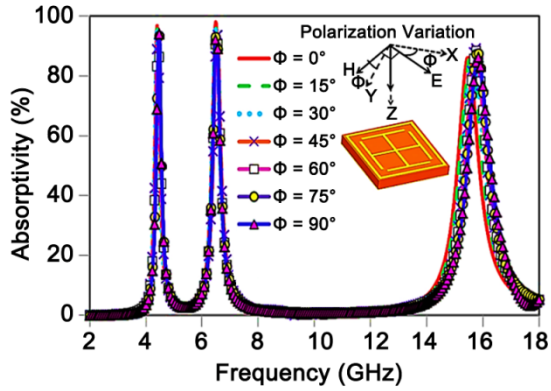

Fig. 3 — Simulated absorptivity for different polarization angles (ϕ) under normal incidence.

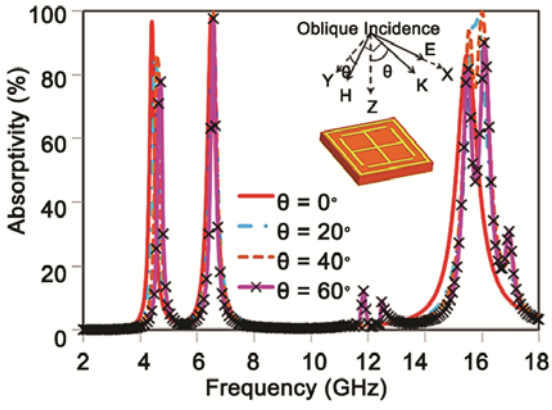

Fig. 4 — Simulated absorptivity for different oblique angles (θ) under TE polarization.

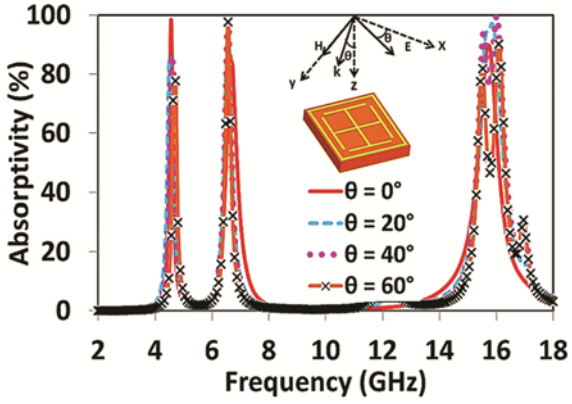

Fig. 5 — Simulated absorptivity for different oblique angles (θ) under TM polarization.

The dimension L_1 of the inner JCS resonator has been varied from 3 mm to 5 mm as shown in Fig. 8(a). It is observed that for L_1 equals to 3 mm the second (f_2) and third (f_3) absorption peaks are at 7.98 GHz and 23.04 GHz, respectively, while for L_1 equals to 5 mm the second and third absorption peaks are at 6.48 GHz and 15.44 GHz, respectively. The variation in dimension of L_1 largely affects the second and third absorption frequencies as the increase in L_1 increases the effective inductance of the inner JCS resonator, thereby the absorption frequencies, i.e., f_2 and f_3 decrease. On the other hand the variation in width W has minor effects on the absorption frequencies as shown in Fig. 8(b). Thus f_2 and f_3 can be controlled by controlling the length L_1. The individual control of f_2 and f_3 can also be achieved by separately controlling the dimensions of the portion I and II of the inner JCS resonator as shown in Fig. 9(a). Hence, the variations of length 'L_1' of the portion I and II is required to be studied so that the proposed design is useful for distinct frequencies in C, X and Ku bands.

Therefore, in order to investigate the individual control of f_2 and f_3 the L_1 dimension of the portion I and II of the inner JCS resonator have been separately

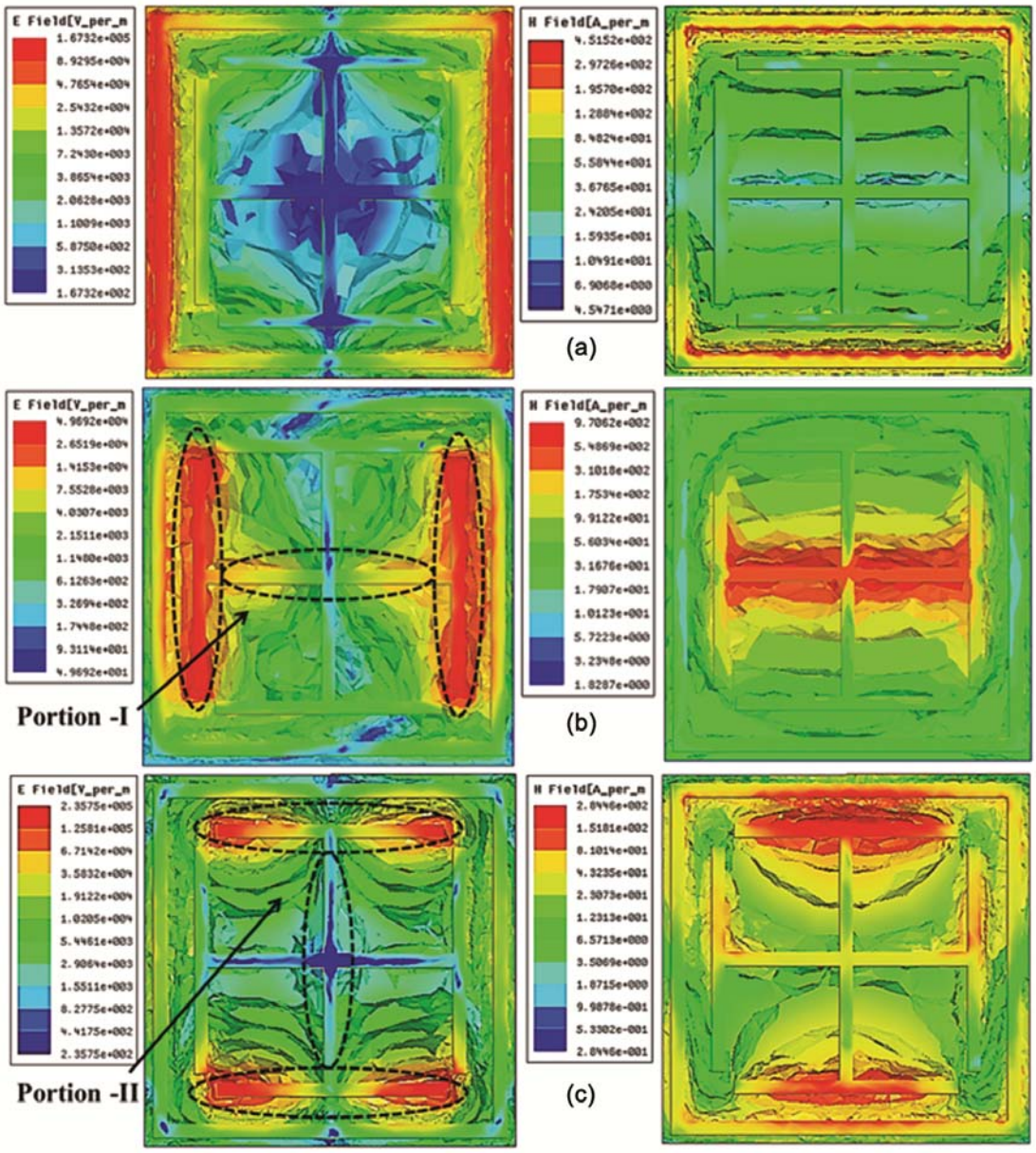

Fig. 6 — Electric and magnetic field distributions at (a) 4.4 GHz (b) 6.48 GHz and (c) 15.44 GHz.

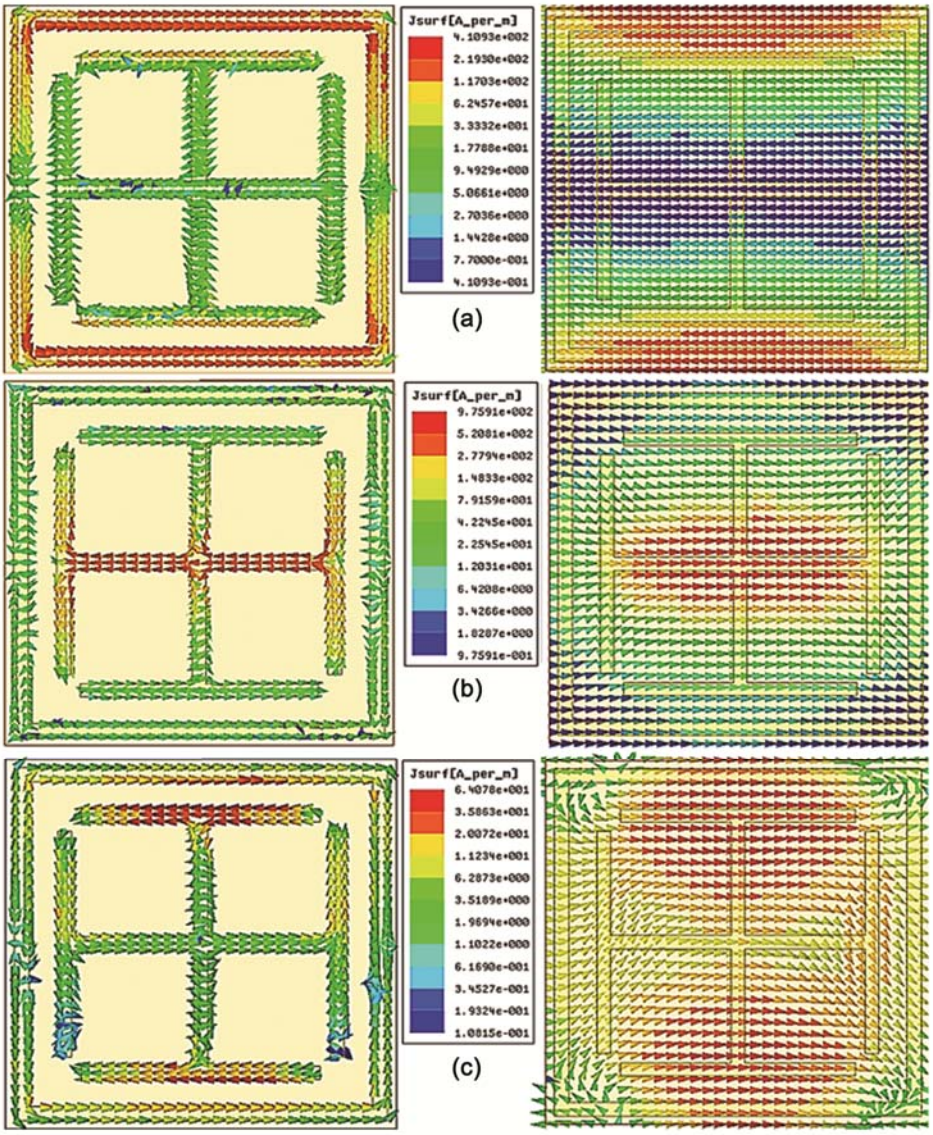

Fig. 7 — Surface current distributions at top and bottom surfaces for (a) 4.4 GHz (b) 6.48 GHz (c) 15.44 GHz.

varied. The variations in absorptivity and the absorption frequencies, i.e., f_2 and f_3 corresponding to different L_1 dimensions of the portion I and II have been listed in Table 1. The absorptivity responses for different L_1 dimensions for portion I and II have been shown in Fig. 9(b,c). It is observed that the second absorption frequency, i.e., f_2 can be adjusted from *C* band to *X* band by varying the dimension L_1 of portion I from 5 mm to 2 mm and third absorption frequency f_3 can be adjusted from *X* band to *Ku* band by varying L_1 of the portion II from 7 mm to 4 mm. This proves that the proposed absorber provides the flexibility to separately control the individual absorption frequencies for *C*, *X* and *Ku* bands. Further, the normalized impedance plot of the proposed triple band absorber has been studied as shown in Fig. 10. For the three absorption frequencies, the real and imaginary values of the impedance as represented through small dotted circles in Fig. 10 have been listed in Table 2. It is observed that the real part of impedance at the three absorption frequencies is near to unity while the imaginary part is near the value zero. Therefore, it implies that there is no reflection from the absorber structure at the optimized frequencies, i.e., f_1, f_2 and f_3 as reported in[13,14].

5 Results and Discussion

For the experimental verification of the performance of the proposed absorber a prototype array of 36×36 elements of the basic structure has been

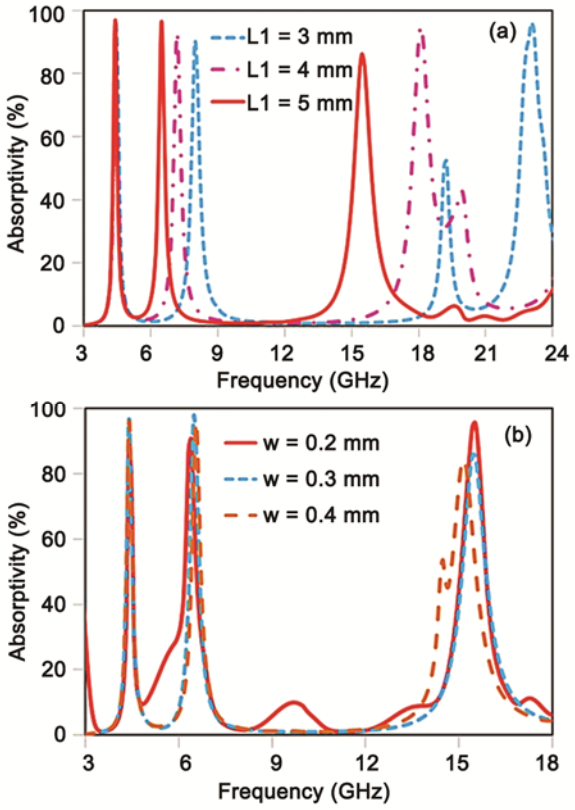

Fig. 8 — Simulated absorptivity for different (a) L_1 and (b) W dimensions.

Table 1 — Effect of variation of L_1dimension on the absorption frequencies f_2 and f_3 for portion I and II of the inner JCS resonator.

Portion I			Portion II		
L_1 (mm)	f_2 (GHz)	Absorptivity (%)	L_1 (mm)	f_3 (GHz)	Absorptivity (%)
5.0	6.48	97.64	7.0	11.12	81.08
4.0	7.12	95.59	6.0	13.04	86.04
3.0	8.08	93.90	5.0	15.44	87.44
2.0	9.60	90.01	4.0	18.20	96.60

fabricated as shown in Fig. 11. The measurements are performed as suggested in literature[13]. Agilent's vector network analyzer (VNA) (Model No. N5222A) connected to two UWB horn antennae of frequency range 1 to 18 GHz is used for experimental measurements as shown in Fig. 12. One of the horn antennas is used as transmitting antenna and the other is used as receiving antenna. Initially, in order to calibrate the test environment the reflection from a copper sheet of identical dimensions (as that of the fabricated prototype array) is measured by placing it in front of the UWB horn antennas at a distance in free space at which near field effects are negligible.

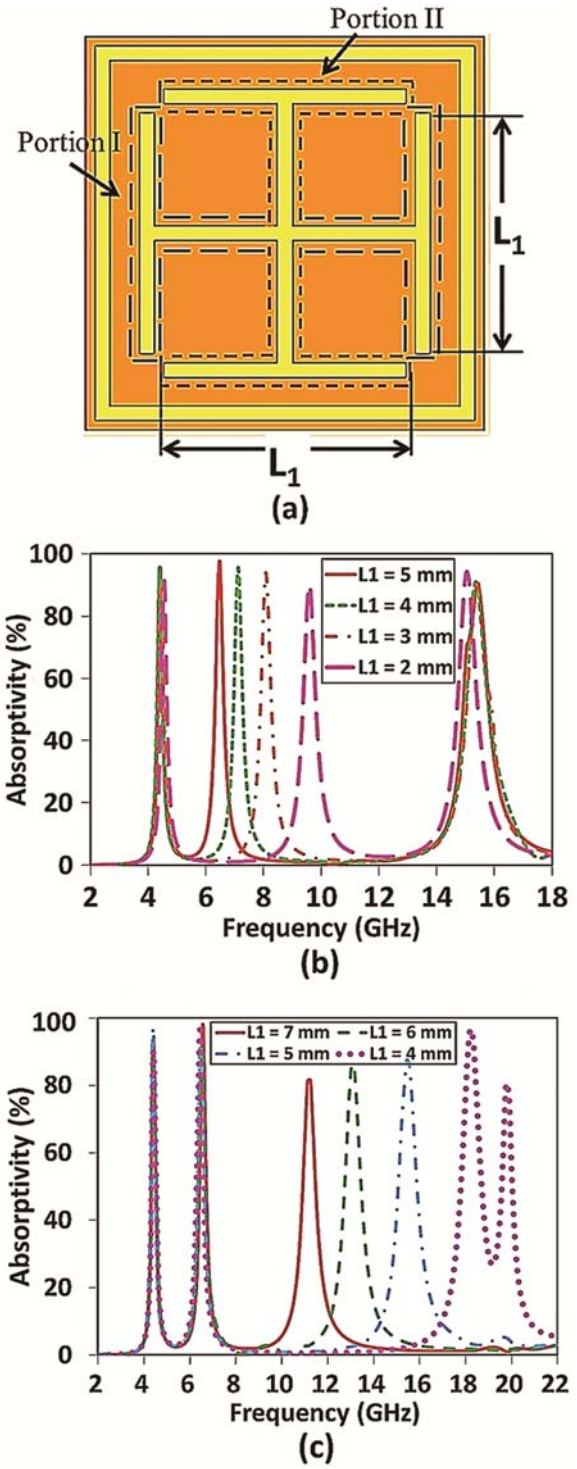

Fig. 9 — (a) Portion I and II of the inner JCS resonator of the proposed absorber and simulated absorptivity for different L_1 dimensions of (b) portion I and (c) portion II.

Then, the copper sheet is replaced by the fabricated structure and the reflected power is measured. This reflected power is subtracted from that of the copper

sheet to evaluate the actual reflection from the fabricated prototype. From this actual reflection, absorptivity is calculated by using the Eq. (1) as reported in literature[13,14].

Table 2 — Real and imaginary parts of normalized input impedance of proposed triple band absorber at f_1, f_2 and f_3.

Absorption frequencies (GHz)	Normalized impedance	
	Real part	Imaginary part
f_1 = 4.4	1.154	-0.254
f_2 = 6.48	0.945	0.084
f_3 = 15.44	1.918	-0.130

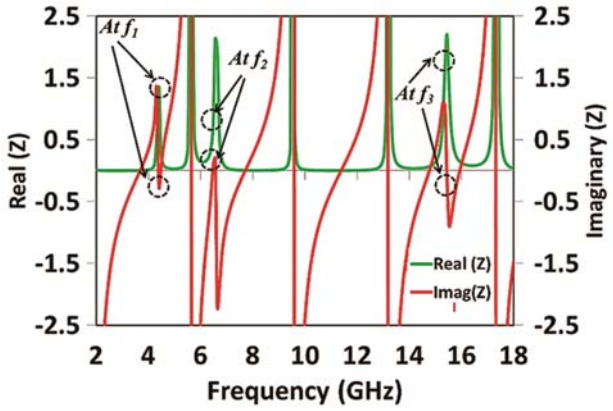

Fig. 10 — Normalized input impedance of the proposed triple band absorber.

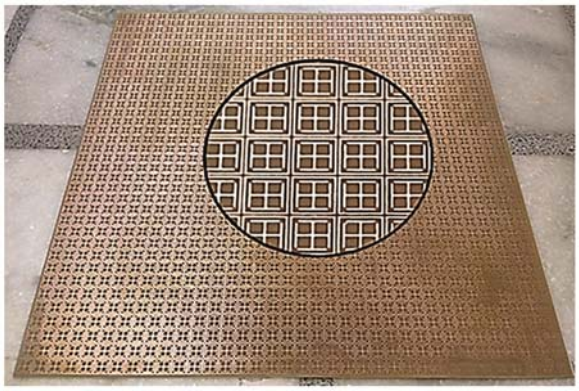

Fig. 11 — Fabricated prototype.

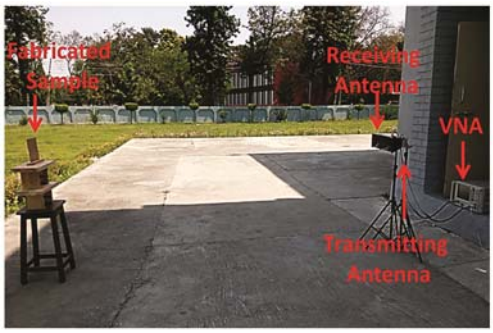

Fig. 12 — Experimental setup.

The comparison of simulated and measured absorptivities has been shown in Fig. 13. The measured response shows that the absorption occurs at 4.48 GHz, 6.56 GHz and 15.76 GHz with absorptivity values of 91.61%, 95.92% and 95.30%, respectively. The small difference between simulated and measured results may be due the nonlinear behaviour of dielectric substrate at higher frequencies and fabrication errors. The fabricated structure has also been experimentally tested both for different angles of polarization under normal incidence as shown in Fig. 14. For this the fabricated structure has been rotated about its axis in steps of 30° from 0° to 60°. The measured response for different polarization angles up to 60° has been shown in Fig. 13. It observed that the proposed absorber is polarization insensitive. Further, the performance of the absorber structure has been experimentally tested for oblique angles of the incident wave. For this the UWB horn antennas are rotated in the steps of 20° from 0° to 60° along the circumference of a circle at the centre of which the fabricated prototype is placed.

The radius of this circle is equal to the far field distance. The measured responses for different

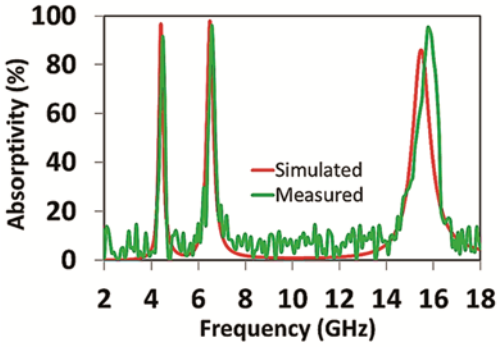

Fig. 13 — Comparison of simulated and measured absorptivity under normal incidence.

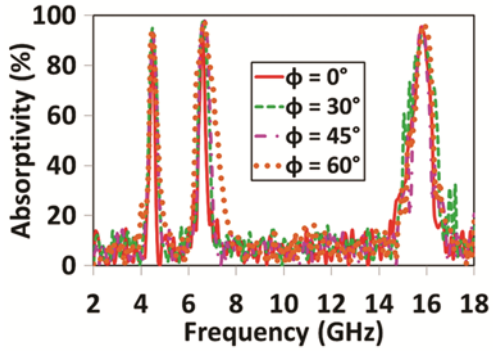

Fig. 14 — Measured absorptivity for different angles (ϕ) of polarization under normal incidence.

oblique incidence angles under TE and TM polarizations have been shown in Fig. 15 and Fig. 16, respectively. It is observed that the proposed absorber exhibits above 80% absorption up to 60° at all the three absorption frequencies for both the polarizations.

Further, the proposed absorber has also been compared with the already existing triple band metamaterial absorbers in terms of unit cell size and thickness at their lowest frequencies of absorption as listed in Table 3. It is observed that in comparison to already reported dual/triple band metamaterial absorbers[11–16] the proposed absorber is compact in its unit cell size (0.12 λ_0) and ultrathin in thickness (0.014 λ_0).These features make it suitable for conformal planar RF applications.

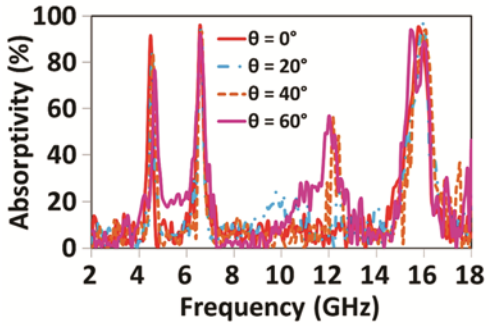

Fig. 15 — Measured absorptivity for different incidence angles (θ) under TE polarization.

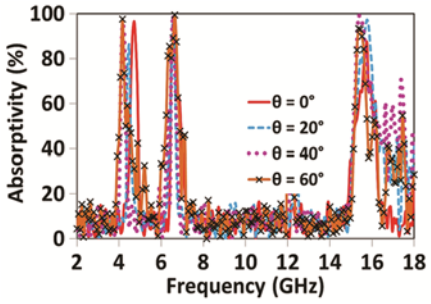

Fig. 16 — Measured absorptivity for different incidence angles (θ) under TM polarization.

Table 3 — Comparison of proposed absorber with already reported triple band absorber designs.

Absorber	Lowest frequency (GHz)	Unit cell size (mm)/ (with respect to lowest frequency)	Thickness (mm)/ (with respect to lowest frequency)
Literature[11]	7.44	15.0 (0.372 λ_0)	1.0 (0.024 λ_0)
Literature[12]	2.09	10.6 (0.073 λ_0)	3.0 (0.020 λ_0)
Literature[13]	5.22	18.0 (0.312 λ_0)	1.0 (0.017 λ_0)
Literature[14]	4.74	18.0 (0.284 λ_0)	1.0 (0.015 λ_0)
Literature[15]	4.88	14.0 (0.227 λ_0)	1.0 (0.016 λ_0)
Literature[16]	8.0	9.0 (0.240 λ_0)	0.8 (0.021 λ_0)
Proposed	4.40	8.2(0.120 λ_0)	1.0 (0.0146 λ_0)

6 Conclusions

A polarization insensitive ultrathin (~λ_0/20) compact triple-band metamaterial absorber has been presented with a Jerusalem cross resonator concentric with an outer square loop resonator. The simulation response shows high absorptivity at the three frequencies of 4.4 GHz, 6.48 GHz and 15.44 GHz. The measured response is in good agreement with simulation one. The proposed absorber can exhibit individual control for its absorption frequencies from *C*-band to *Ku*-band. The physical mechanism of absorption has been investigated by using field and surface current distributions. The absorption characteristics of the proposed absorber for different polarization and oblique incidence angles have also been validated through both simulation and experimental investigations. The proposed design is compact in size and ultrathin in thickness as compared to the already reported dual/triple band absorbers. Therefore, the proposed absorber is a good candidate for the design of multiband absorbers and can be used for potential applications such as stealth technology and in reduction of electromagnetic interference etc.

Acknowledgement

The work was supported by funding of TEQIP-II (subcomponent 1.1) project for graduate studies and research. The authors want to thank the officials and staff of the Vidyut Yantra Udyog, Modinagar (UP), India, for their kind support in fabricating the structure. The authors are also thankful to Mr Saptarshi Ghosh, (Ph D Scholar, IIT Kanpur, India) for his valuable suggestions in experimental measurements.

References

1 Smith D R, Padilla W J, Vier D C, Nemat-Nasser S C & Schultz S, *Phys Rev Lett*, 84 (2000) 4184.
2 Schurig D, Mock J J, Justice B J, Cummer S A, Pendry J B, Starr A F & Smith D R, *Science*, 314 (2006) 977.
3 Fang N, Lee H, Sun C & Zhang X, *Science*, 38 (2005) 534.
4 Enoch S, Tayeb G & Vincent P, *Phys Rev Lett*, 89 (2002) 3901.
5 Noor A & Hu Z, *IET Microwave Antennas Propag*, 4 (2010) 667.
6 Landy N I, Sajuyigbe S, Mock J J, Smith D R & Padilla W J, *Phys Rev Lett*, 100 (2008) 207402.
7 Luukkonen O, Costa F, Simovski C R, Monorchio A & Tretyakov S A, *IEEE Trans Antennas Propag*, 57 (2009) 3119.
8 Ye Q, Liu Y, Lin H, Li M & Yang H, *Appl Phys A*, 107 (2012) 155.

9 Wen Q Y, Zhang H W, Xie Y S, Yang Q H & Liu Y L, *Appl Phys Lett*, 95 (2009) 241111.
10 Zheng D, Cheng Y, Cheng D, Nie Y & Gong R, *Prog Electromagn Res*, 142 (2013) 221.
11 Li H, Yuan L H, Zhou B, Shen X P & Cheng Q, *J Appl Phys*, 110 (2011) 014909.
12 Xu H X, Wang G M, Qi M Q, Liang J G, Gong J Q & Xu Z M, *Phys Rev B*, 86 (2012) 205104.
13 Bhattacharyya S, Ghosh S & Srivastava K V, *J Appl Phys*, 114 (2013) 094514.
14 Bhattacharyya S & Srivastava K V, *J Appl Phys*, 115 (2014) 064508.
15 Wang G D, Chen J F, Hu X W, Chen Z Q & Liu M H, *Prog Electromagn Res*, 145 (2014) 175.
16 Ayop O, Rahim M K A, Murad N A, Samsuri N A & Dewan R, *Prog Electromagn Res*, 39 (2014) 65.
17 Zhai H, Zhan C, Li Z & Liang C, *IEEE Antennas Wireless Propag Lett*, 14 (2015) 241.
18 Huang L & Chen H, *Prog Electromagn Res*, 113 (2011) 103.